Civil Engineering and Applied Solutions

Research Article

journal homepage: ceas.journals.umz.ac.ir

Performance-Based Seismic Assessment of RC Frames Strengthened with Steel Angle and Strap Systems

Hananeh Dashtaki [a], Javad Shayanfar [b*], Morteza Jamshidi [a]

[a] *Department of Civil Engineering, Cha. C., Islamic Azad University, Chalous, Iran*
[b] *Department of Civil Engineering, University of Minho, Azurém, Guimarães 4800-058, Portugal*

ARTICLE INFO

Article history:

Received 25 February 2026

Revised 10 April 2026

Accepted 16 June 2026

Available online 01 April 2027

Keywords:

Reinforced concrete frames

Seismic retrofit

Steel angles and straps

Nonlinear analysis

ABSTRACT

The seismic vulnerability of reinforced concrete (RC) structures designed according to outdated standards lacking seismic provisions has been widely documented through experimental investigations and post-earthquake observations. Consequently, reliable assessment of the seismic performance of such structures and the development of effective strengthening strategies remain critical objectives in earthquake engineering. This study investigates the seismic behavior of RC frames strengthened using steel angle and strap systems through analytical and numerical approaches. A novel sectional moment-curvature model is developed, incorporating confinement effects from stirrups and steel straps as well as local buckling of compressive steel angles. Sectional curvature is converted to member rotation to derive plastic hinge properties for nonlinear structural analysis. The proposed model is validated against experimental data from existing studies, demonstrating strong agreement in predicting flexural and shear behavior. Subsequently, the seismic performance of strengthened RC members and structural systems is evaluated through nonlinear pushover analysis, with emphasis on performance levels, plastic hinge development, and failure mechanisms. Results indicate that the steel angle and strap system substantially enhances load-carrying capacity and ductility, leading to improved seismic performance and reduced structural vulnerability. These findings confirm the effectiveness of the strengthening strategy and provide an analytical framework for performance-based seismic assessment and retrofit design of existing RC structures.

How to cite this article: Dashtaki, H., Shayanfar, J., Jamshidi, M. Performance-Based Seismic Assessment of RC Frames Strengthened with Steel Angle and Strap Systems. Civil Engineering and Applied Solutions. 2027; 3(2): 49–68. doi:10.22080/ceas.2026.31395.1082.

Nomenclature

Parameter	Description	Parameter	Description
A_g	Total area of the section	t_1	Thickness of steel angles
A_{con}	Areas of confined regions	t_2	Thickness of steel straps
A_{unc}	Areas of unconfined regions	v	Poisson's ratio
A_{s1}	Area of steel bars at tension	V_{ang}	Shear strength due to steel angles
A_{s2}	Area of steel bars at compression	V_{bat}	Shear strength due to steel straps
b	Smaller width of the section	v_c	Shear stress capacity in compression
c	Neutral axis	v_t	Shear stress capacity in tension
C_{con}	Concrete compressive force	v_n	Shear capacity due to concrete
d_b	Diameter of steel bars	V_n	Total shear strength

* Corresponding author.
E-mail addresses: arch3d.ir@gmail.com (J. Shayanfar).

https://doi.org/10.22080/ceas.2026.31395.1082
ISSN: 3092-7749/© 2027 The Author(s). Published by University of Mazandaran.

E_c	Unconfined concrete elastic modulus	x	Axial strain ratio
E_{sec}	Modulus of unconfined concrete at the peak	α_1	Empirical factor for confinement-induced gain
E_s	Steel elastic modulus	α_2	Empirical factor for non-circularity effects
f_c	Concrete axial stress	φ	Curvature
f_c'	Peak strength of unconfined concrete	φ_y	Yield curvature
$f_{cc,sj}'$	Peak strength of confined concrete	φ_u	Ultimate curvature
f_j	Confining stress of steel straps	θ_i	Rotation
f_l	Minimum confinement pressure	θ_{bb}	Ultimate rotation capacity
F_l	Maximum confinement pressure	θ_{p_bb}	Plastic rotation threshold
f_s	Confining stress of steel stirrups	ε_0	Axial strain at the peak stage
F_{sa}	Axial stress at steel angles	ε_c	Axial strain
f_t	Concrete tensile strength	$\varepsilon_{cc,sj}$	Axial strain at the peak stage
f_{ya}	Yield stress of the steel angles	ε_l	Lateral/hoop strain
f_{ys}	Yield stress of steel stirrups	ε_s	Tensile strain in steel bars
h	Larger width of the section	ε_{sa}	Axial strain at steel angles
K_e	Confinement effectiveness factor	ε_{sb}	Yield strain of steel straps
$K_{e,j}$	Confinement effectiveness factor	ε_{sy}	Yield strain of steel stirrups
L_1	Width of steel angles	ε_{ya}	Yield strain of steel angles
L_2	Width of steel straps	ρ_{jx}	Strap reinforcement ratio in x direction
L_{eff}	Effective column length	ρ_{jy}	Strap reinforcement ratio in y direction
L_p	Plastic hinge length	ρ_{sx}	Stirrup reinforcement ratio in x direction
M_f	Bending capacity	ρ_{sy}	Stirrup reinforcement ratio in y direction
M_n	Equivalent bending capacity	ρ_t	Total longitudinal reinforcement ratio
N	Applied axial load	σ	Normal stress
N_{max}	Maximum axial capacity	σ_c	Principal compressive stress
n_c	Local buckling-induced reduction	σ_t	Principal tensile stress
s'	Steel stirrup spacing	t_1	Thickness of steel angles
s_b	Steel strap spacing	t_2	Thickness of steel straps

1. Introduction

Evidence from past earthquakes, as well as numerous experimental and analytical studies [1-3] , clearly demonstrates the seismic vulnerability of reinforced concrete (RC) structures that were inadequately designed according to outdated codes. It is noteworthy that a significant portion of existing RC structures worldwide were constructed prior to the development and enforcement of modern seismic design codes; consequently, the seismic provisions embedded in contemporary codes were not considered in their original design [4, 5]. Therefore, in order to enhance the seismic performance of existing structures and align them with current performance-based requirements, it is first essential to identify structural weaknesses and accurately assess seismic behavior, and subsequently, if necessary, to implement an appropriate strengthening strategy.

In recent years, one of the retrofitting methods that has gained considerable attention from researchers and practicing engineers is the use of steel angle and strap (or batten) systems. This system not only significantly improves the seismic performance of members and the overall structure, but also offers advantages such as cost-effectiveness, ease of material availability, and relatively rapid and straightforward implementation [6-12]. Experimental studies by Salman and Al-Sherrawi [6] on RC columns strengthened with steel angle and strap systems under lateral loading demonstrated that this retrofitting method enhances the flexural behavior of members and substantially increases energy dissipation capacity. Montuori and Piluso [13] and Nagaprasad et al. [14] further evaluated the performance of the system through tests on eccentrically loaded strengthened columns. Their results indicated that the steel angle and strap system increases flexural strength through the participation of steel angles in resisting tensile and compressive forces, while simultaneously improving member ductility by enhancing confinement pressure provided by the straps. Campione et al. [15] focused on analytical modeling and proposed a model to estimate the flexural and shear capacity of RC columns strengthened with steel angle and strap systems. In this model, the compatibility of strains between the angles and concrete was neglected to account for shear stresses, resulting in a more conservative and safer prediction of structural behavior. Moreover, Campione [16], through a numerical study, examined the effect of steel angles and straps on the strength and ductility of RC columns, demonstrating that reducing the spacing between straps not only increases strength within the axial load-moment interaction domain but also significantly improves the ductility of strengthened members due to enhanced lateral confinement, as also confirmed by Shhatha et al. [9], Hu et al. [10], Campione [17], Badalamenti et al. [18].

The novelty of this study lies in the development of an integrated nonlinear analytical model that explicitly captures the coupled behavior of flexure, shear, confinement, and instability mechanisms in RC members strengthened with steel angle and strap systems.

At the material level, the model extends conventional confined concrete formulations by incorporating the combined and direction-dependent confinement effects of stirrups and external steel straps through an iterative procedure for determining effective lateral pressure. At the sectional level, it introduces a unified fiber-based moment-curvature framework in which steel angles are fully integrated into strain compatibility and force equilibrium, while their compressive behavior includes local buckling effects, enabling realistic prediction of post-peak response. Furthermore, the model explicitly couples flexural deformation with shear capacity degradation by updating shear resistance as a function of member rotation and accounting for contributions from concrete, stirrups, steel straps, and angles. The bar buckling formulation is also extended to include the influence of external confinement. Importantly, unlike existing studies that are generally limited to member-level or uncoupled formulations, this work provides a consistent framework that captures coupled flexure-shear-confinement behavior and applies it from the sectional level to full structural analysis. To the best of the authors' knowledge, such a comprehensive and unified modeling approach for steel angle and strap strengthening systems, validated at both member and structural levels, has not been previously reported.

The paper first describes the strengthening system and the underlying modeling assumptions, followed by the development of the nonlinear analytical framework, including material constitutive relationships and sectional analysis procedures. The proposed model is then validated against available experimental results, and subsequently employed to assess the seismic response of multi-story RC frames before and after strengthening. Finally, the key findings are discussed, and the main conclusions are drawn.

2. Steel angle and strap strengthening method

The strengthening system investigated in this study consists of steel angles installed at the corners of columns, which are interconnected by steel straps (or batten). This system, by establishing a combined confinement and structural participation mechanism, can effectively enhance the seismic performance of RC members.

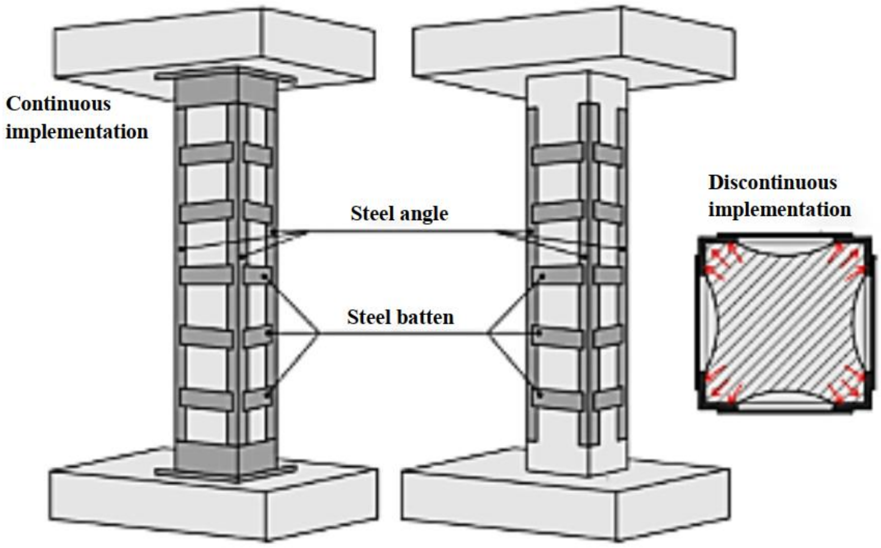

Fig. 1. Configuration of the steel angle and strap strengthening system.

The main advantages of the steel angle and strap system can be summarized in three key aspects:

1. Increased lateral confinement pressure on the concrete core, leading to a significant improvement in member ductility;
2. Enhanced shear capacity and, when properly designed, the potential to shift the failure from brittle shear to ductile flexure;
3. Provision of axial resistance (tension and compression) through the steel angles, which subsequently increases the flexural capacity of the column section.

The effectiveness of the steel angle and strap system is directly dependent on the execution and quality of component connections. When the system is implemented in a discontinuous manner (as shown in Fig. 1), the steel straps primarily serve to provide lateral confinement, and the improvement in member behavior is reflected in enhanced strength and ductility [5]. In this case, due to the lack of effective force transfer, the steel angles do not actively participate in resisting tensile and compressive forces. In contrast, with continuous implementation of the strengthening system (Fig. 1), the steel angles actively contribute to the flexural behavior of the member by resisting both tensile and compressive forces, in addition to the ductility enhancement provided by concrete confinement. Therefore, the selection of appropriate detailing and ensuring proper continuity between the steel components and the RC member play a decisive role in the effectiveness of this strengthening method.

3. Steel angle and batten strengthening method

In this section, the methods used to determine the nonlinear behavior of RC members strengthened with the steel angle and strap system are described. Based on the discrete plastic hinge approach [19], the properties of RC members in the moment-rotation relationship can be determined through sectional moment-curvature analysis and the subsequent conversion of curvature to rotation. To perform this analysis, it is essential to define the nonlinear behavior of the materials used in the member; therefore, the method for calculating material properties is presented below.

3.1. Confined concrete with stirrups and steel batten

The steel angle and strap strengthening system, in addition to the transverse reinforcement in the section, can enhance concrete behavior by increasing the confinement pressure [6, 8, 20]. The elevated confinement pressure results in improved strength and ductility of the reinforced concrete members, with detailed information of its mechanism that can be found in Shayanfar et al. [21], Shayanfar et al. [22], Shayanfar et al. [23]. In Fig. 2, the regions of an RC member section subjected to confinement pressure from the steel angle and strap strengthening system, as well as transverse reinforcement, are illustrated.

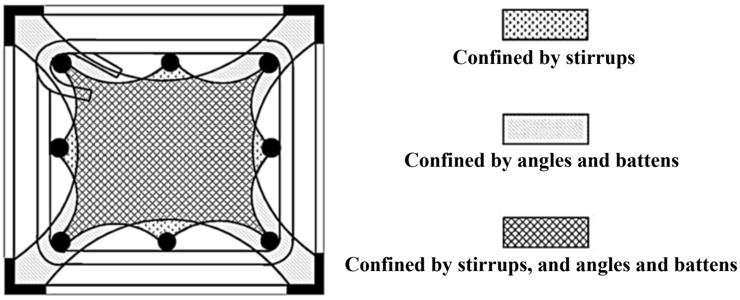

Fig. 2. Sectional regions exposed to confinement provided by angle and batten system as well as stirrups.

As can be observed in Fig.2, the cross-section of a reinforced concrete member strengthened with a steel angle and steel strip system can be divided into two regions based on the confinement pressure [24-26]: (I) Regions subjected to confinement pressure from the steel angles and steel strips; (II) Regions subjected to confinement pressure from the steel angles and steel strips in combination with the transverse reinforcement. However, in this paper, for the sake of conservatism and simplicity, the confined regions located outside the core of the section, which are confined by the aforementioned strengthening system, have been neglected. The details of the strengthening system under investigation are illustrated in Fig. 3. The parameters t_1 and t_2 denote the thicknesses of the steel angles and steel strips, respectively. The remaining parameters are shown and can be identified in Fig. 3.

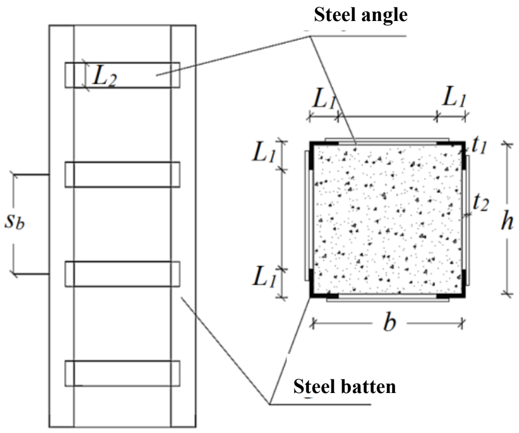

Fig. 3. Specimen of a reinforced concrete column strengthened with a steel angle and batten system.

In this study, the axial stress-strain model for concrete proposed by Mander et al. [27], with some modifications, has been adopted to account for the confinement effect by the steel angle and batten system. The formulation can be expressed as Eq. 1.

$$f_c = \frac{f'_{cc,sj} x r}{r-1+x^r} \tag{1}$$

where:

$$x = \frac{\varepsilon_c}{\varepsilon_{cc,sj}} \tag{2}$$

$$r = \frac{E_c}{E_c - E_{sec}} \tag{3}$$

$$E_{sec} = \frac{f'_{cc,sj}}{\varepsilon_{cc,sj}} \tag{4}$$

$$\varepsilon_{cc,sj} = \varepsilon_0 \left[1 + 5\left(\frac{f'_{cc,sj}}{f'_c} - 1\right)\right] \tag{5}$$

Here, E_c is the concrete elastic modulus; f'_c and ε_0 are the axial stress and strain at the peak stage of unconfined concrete. The maximum compressive strength ($f'_{cc,sj}$) of concrete confined by the steel angle and strap strengthening system, as well as transverse reinforcement, corresponds to $\varepsilon_{cc,sj}$ and can be calculated by Eq. 6.

$$f'_{cc,sj} = \alpha_1 \alpha_2 f'_c \tag{6}$$

where:

$$\alpha_1 = 2.254\sqrt{1+\frac{7.94F_l}{f'_c}} - 2\frac{F_l}{f'_c} - 1.254 \tag{7}$$

$$\alpha_2 = \left(1.4\frac{f_l}{F_l} - 0.6\left(\frac{f_l}{F_l}\right)^2 - 0.8\right)\sqrt{\frac{F_l}{f_l}} + 1 \tag{8}$$

In Eq. 1, α_2 is used to account for the effect of varying lateral confinement in the vertical and horizontal directions of the section, following the study by Wang and Restrepo [28]. In this equation, f_l and F_l represent the minimum and maximum effective lateral confinement pressures, respectively, which can be calculated by Eqs. 9 and 10.

$$f_l = min(f_{l,sx} + f_{l,jx}, f_{l,sy} + f_{l,jy}) \tag{9}$$

$$F_l = max(f_{l,sx} + f_{l,jx}, f_{l,sy} + f_{l,jy}) \tag{10}$$

where:

$$f_{l,sx} = K_e\rho_{sx}f_s \tag{11}$$

$$f_{l,sy} = K_e\rho_{sy}f_s \tag{12}$$

$$f_{l,jx} = K_{e,j}\rho_{jx}f_j \tag{13}$$

$$f_{l,jy} = K_{e,j}\rho_{jy}f_j \tag{14}$$

In the above equation, ρ_{sx} and ρ_{sy} denote the ratios of transverse reinforcement in the horizontal and vertical directions of the section, respectively. Similarly, ρ_{jx} and ρ_{jy} represent the ratios of steel straps in the horizontal and vertical directions, respectively. The parameter f_j and f_s corresponds to the lateral confining stress induced by the steel straps and transverse reinforcement. In addition, the coefficients K_e and $K_{e,j}$ represent the confinement effectiveness factors associated with the transverse reinforcement and the steel angle and strap strengthening system, respectively, whose values are determined by Eqs. 15 and 16.

$$K_e = \frac{\left(1-\sum_{i=1}^{n}\frac{w_i{}^2}{6bh}\right)\left(1-\frac{s\prime}{2b}\right)\left(1-\frac{s\prime}{2h}\right)}{1-\rho_t} \tag{15}$$

$$K_{e,j} = \frac{\left(1-\rho_t-\{(h-2L_1)^2+(b.-2L_1)^2\}\right)}{3A_g(1-\rho_t)} \times \left(1-\frac{s_b-L_2}{2h}\right)\left(1-\frac{s_b-L_2}{2b}\right) \tag{16}$$

The parameter w_i denotes the clear spacing between adjacent longitudinal reinforcing bars. In addition, A_{sv} and A_g represent the total area of transverse reinforcement and the gross cross-sectional area, respectively. The ratio ρ_t corresponds to the longitudinal reinforcement ratio with respect to the gross sectional area. To determine the lateral confining pressure corresponding to the maximum compressive strength of concrete, a novel procedure is proposed, which is described in the following section.

1. Assume an initial value for the axial strain of concrete ε_a.
2. Convert the axial concrete strain to the corresponding lateral strain (parallel to the member cross-section) in the steel straps and transverse reinforcement, ε_l, assuming a Poisson's ratio equal to 0.5 [29, 30].
3. Calculate the stress developed in the steel batten.
4. Calculate the stress developed in the transverse reinforcement.
5. Determine the lateral confinement pressure induced by the steel angle and batten system using Eqs. 13 and 14.
6. Determine the lateral confinement pressure provided by the transverse reinforcement using Eqs. 11 and 12.
7. Calculate the maximum compressive strength of concrete based on Eq. 6.
8. Determine the axial strain corresponding to the maximum compressive strength of concrete using Eq. 5.
9. Compare the assumed axial strain in Step (1) with the axial strain obtained in Step (8).

$$\varepsilon_l = 0.5 \times \varepsilon_a \tag{17}$$

$$f_j = E_j \times \varepsilon_l \qquad \varepsilon_l \le \varepsilon_{yb} \tag{18}$$

$$f_j = f_{yj} \qquad \varepsilon_l > \varepsilon_{yb} \tag{19}$$

$$f_{s,j} = E_s \times \varepsilon_l \qquad \varepsilon_l \le \varepsilon_{sy} \tag{20}$$

$$f_{s,j} = f_{ys} \qquad \varepsilon_l > \varepsilon_{sy} \tag{21}$$

If the axial strain assumed in Step (1) shows adequate convergence with the value obtained in Step (8), the concrete stress-strain behavior can be evaluated using Eq. 1, based on the maximum compressive strength determined in Step (7) and the corresponding axial strain obtained in Step (8). Otherwise, a new value for the axial strain is assumed in Step (1), and the calculation procedure is repeated until convergence is achieved.

3.2. Local buckling of compressed steel angles

Based on previous studies [13, 14, 18, 20, 31], the effects of local buckling must be considered in the moment-curvature analysis of steel angles under compression used in strengthening systems. In the present study, the analytical model proposed by Campione [17] is adopted, which is based on the findings of Badalamenti et al. [18] and accounts for the influence of local buckling on the nonlinear behavior of compressed steel angles. According to this model, the stress-strain relationship of the compressed steel angles is defined by Eqs. 22 and 23.

$$min\left(E_s\varepsilon_s, n_c\, f_{ya}\right) \qquad \varepsilon_s \le \varepsilon_{ya} \tag{22}$$

$$min\left(f_{ya}, n_c\, f_{ya}\right) \qquad \varepsilon_s > \varepsilon_{ya} \tag{23}$$

where:

$$n_c = \frac{1}{\sqrt{2\varepsilon_s - \varepsilon_s^2}}\left\{0.5\frac{L_1 t_1}{s_b t_2}\left(1 - 0.5\frac{R}{f_{ya}}\right) - C\right\} \tag{24}$$

$$R = min\left(\varepsilon_s E_s, f_{ya}\right) \tag{25}$$

$$C = 0.47\frac{E_s\varepsilon_s}{t_2 b f_{ya}}\left(\frac{e^{\left[-1.5\left(\frac{s_b}{b}\right)\right]}}{\left[\frac{L_1}{(s_b t_1)}\right] + \left[\frac{(0.5b - L_1)}{(L_2 t_2)}\right]}\right) \tag{26}$$

where f_{ya} denotes the yield stress of the compressed steel angles corresponding to the compressive strain ε_{ya}. By modifying the stress-strain relationship of the compressed angles, when the local buckling mechanism initiates ($0 < n_c < 1$), a decrease in n_c leads to a reduction in the longitudinal stress and, consequently, the compressive force developed in the steel angles. This reduction in longitudinal stress directly affects the strain compatibility and force equilibrium relationships.

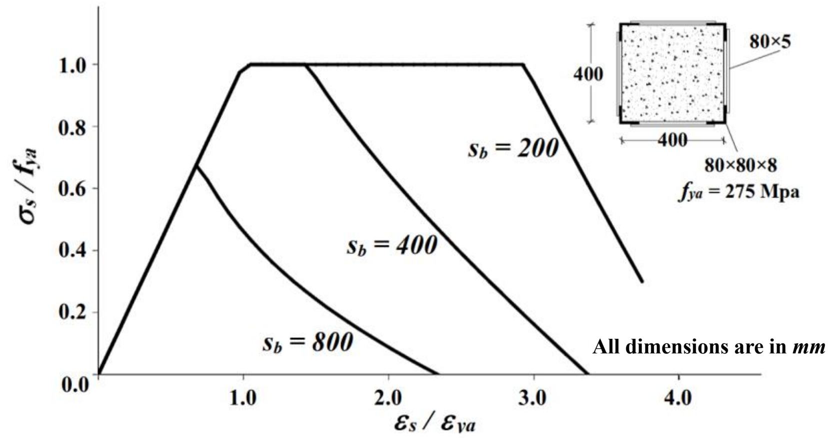

Fig. 4. Longitudinal stress-longitudinal strain relationship of steel angles under compression.

3.3. Moment-curvature analysis

In this section, the theoretical framework and analytical procedure for performing moment-curvature analysis of an RC member strengthened with a steel angle and steel strip system are presented. Moment-curvature analysis is a sectional nonlinear analysis method used to characterize the flexural response of structural members. It establishes the relationship between the applied bending moment and the resulting curvature of the cross-section, thereby enabling evaluation of stiffness degradation, yielding progression, confinement effects, and ultimate flexural capacity.

The method is particularly suitable for composite or strengthened sections, where multiple materials with distinct constitutive laws interact. In the present study, by following Shayanfar et al. [32], Shayanfar et al. [33], Shayanfar et al. [34], a fiber-based sectional modeling approach is employed. In this technique, the cross-section is discretized into numerous small fibers, each assigned an appropriate uniaxial stress-strain relationship according to its material type (confined concrete, unconfined concrete, longitudinal reinforcement, and steel angles). Under the assumptions of strain compatibility and plane sections remaining plane, the strain distribution across the depth of the section is determined from the imposed curvature. The internal forces are then obtained by integrating the stresses over the sectional area, and equilibrium with the applied axial load is enforced to compute the corresponding bending moment [35]. Fig. 5 schematically illustrates the fiber-section model of a reinforced concrete member strengthened with the steel angle and steel strip system. In Fig. 5, F_{sa} and f_{sa} denote the longitudinal force and longitudinal stress in the steel angles at the section level, respectively. The remaining variables, including sectional geometry, strain distribution, and internal force components, are defined within Fig. 5.

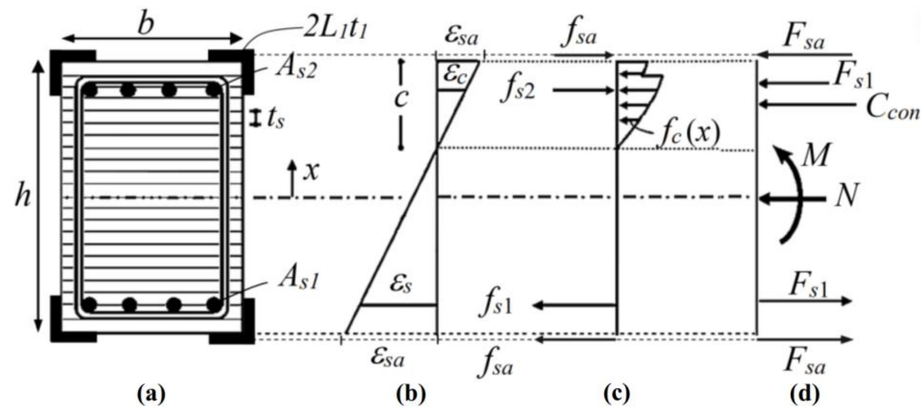

Fig. 5. Fiber analysis of a reinforced concrete member strengthened with a steel angle and steel strip system: (a) cross-section; (b) distribution of longitudinal strains; (c) distribution of longitudinal stresses; and (d) distribution of compressive and tensile forces within the section.

The moment-curvature analysis procedure employed in this study can be summarized as follows:

1. Assume a value for the concrete strain at the extreme fiber of the section.
2. Assume a value for the neutral axis position, c.
3. Calculate the total compressive forces in the concrete, the tensile and compressive forces in the longitudinal reinforcement, and the tensile and compressive forces in the steel angles (Eqs. 27 to 29).

$$C_{con} = \sum f_c(x) b\, t_s \tag{27}$$

$$F_{si} = \sum f_{si} A_{si} \tag{28}$$

$$F_{sa} = \sum 2 f_{sa} L_1 t_1 \tag{29}$$

4. Check the force equilibrium in the section ($C_c + F_{si} + F_{sa} - N\ = 0$). If the sum $C_c + F_{si} + F_{sa}$ is close to the applied axial force, the assumed neutral axis position is correct. Otherwise, a new value for the neutral axis position must be assumed.
5. Calculate the bending moment (Eq. 30), in which d_i and d_{ai} are the distances of the steel bar and steel angles to the top of the section.

$$M_f = \sum f_c(x) b\, t_s x_i + \sum F_{si}\left(\frac{h}{2} - d_i\right) + \sum F_{sa}\left(\frac{h}{2} - d_{ai}\right) \tag{30}$$

6. Curvature Calculation (Eq. 31)

$$\varphi_i = \frac{\varepsilon_c}{c} \tag{31}$$

7. Assume a new value for the concrete strain at the extreme fiber of the section, and repeat the process until the strain in a fiber of the confined region reaches its maximum value.
8. Determine the moment-curvature relationship.

Using the above procedure, the moment-curvature relationship of the RC member strengthened with the steel angle and strap system can be obtained. By converting this relationship into a moment-rotation relationship based on the plastic hinge approach (Fig. 6), the properties of plastic hinges can be derived. The rotation of the RC member corresponding to each curvature level can be calculated by Eqs. 32 and 33).

$$\theta_i = \frac{\varphi_i \times L_{eff}}{2} \qquad \varphi_i < \varphi_y \tag{32}$$

$$\theta_i = \frac{\varphi_y \times L_{eff}}{2} + \left(\varphi_i - \varphi_y\right) \times L_p \qquad \varphi_i \geq \varphi_y \tag{33}$$

where:

$$L_{eff} = L + 0.022 f_s d_b \qquad f_s \leq f_y \tag{34}$$

$$L_p = 0.08L + +0.022 f_y d_b \geq 0.044 f_y d_b \tag{35}$$

Here, φ_y and φ_u represent the yield and ultimate curvature of the transverse reinforcement, respectively. The plastic hinge length of the member, L_p, is calculated based on the relationship proposed by Paulay and Priestly [36]. L is the distance between the maximum and zero moment, produced in the member.

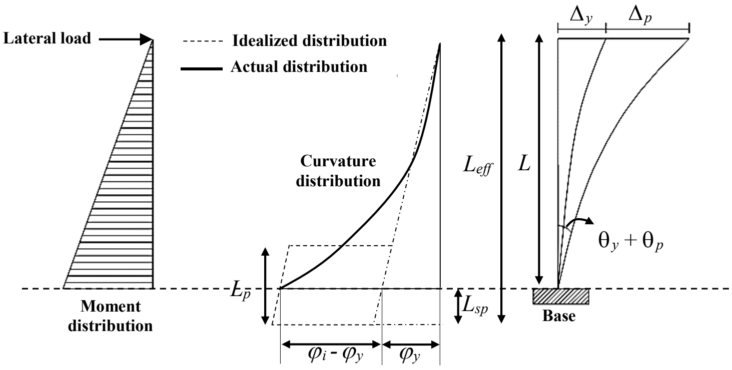

Fig. 6. Plastic hinge approach.

3.4. Shear behavior of RC member with steel angle and batten strengthening method

Insufficient shear capacity in RC members such as beams and columns can lead to nonlinear behavior and a brittle shear failure mechanism [37-39]. The formation of diagonal shear cracks in RC columns and the subsequent reduction in axial load-carrying capacity may cause axial failure of these members, thereby increasing the vulnerability of the structure to seismic actions. Conversely, increased flexural deformations and rotations of the member, accompanied by the development of diagonal tensile cracks, can reduce shear capacity. Under seismic loading, as flexural deformations and rotations increase, after yielding of the longitudinal tensile reinforcement, the width of flexural cracks grows and tensile crushing and cracking of concrete occur in compressive zones of the section [1, 40-42]. Moreover, with the increase in flexural deformations, the height of the neutral axis decreases, which can further reduce the shear capacity of the RC member. Therefore, simulation of the shear mechanism in nonlinear analysis of structural members as a function of flexural deformations is necessary and constitutes one of the objectives of this paper. For a member strengthened with a steel angle and steel strip system, in addition to stirrups and concrete, the steel strips and angles also contribute to the shear capacity of the member. Accordingly, in this study, to determine the contribution of the angles and strips to shear resistance, the model proposed by Campione et al. [15] has been employed, which is expressed in the following equations.

$$V_{angles} = c_1 \frac{{L_1}^2 \times t_1}{2 \times s_b} f_{ya} \tag{36}$$

$$V_{batten} = c_2 \frac{2L_2 \times t_2 \times d}{s_b} f_{yb} \tag{37}$$

where:

$$c_1 = \frac{1}{1 + \left[\left(\frac{L_2}{L_1}\right)^3 \times \frac{t_2 s_b}{t_1 (b - 2L_1)}\right]} \tag{38}$$

$$c_2 = 1 - \frac{N}{N_{max}} \tag{39}$$

In the above equations, f_{yb} represent the yield stresses of the steel angles and steel strips, respectively. N_{max} denotes the maximum axial capacity of the member strengthened with the steel angle and steel strip system, which in this study is calculated by Eq. 40.

$$N_{max} = f'_{cc}\, A_{con} + 0.85 f'_c\, A_{unc} + f_y A_{st} + 8 n_a f_{ya} L_1 t_1 \tag{40}$$

In which, based on studies by Campione [15-17]:

$$0 \le n_a = \frac{1}{2 f_{ya} L_1 t_1} \sqrt{4 L_1 f_{ya} \left({L_1}^2 t_1 f_{ya} - 2\sqrt{2} \frac{L_2 t_2 s_b f_{yb}}{3 L_1} e^{\left(-1.5 \frac{s_b}{b}\right)}\right)} \le 1 \tag{41}$$

In the above relations, A_{con} and A_{unc} denote the areas of confined and unconfined regions, respectively. The coefficient n_a accounts for the effects of angle buckling on the compressive force contributed by the angles. To determine the concrete contribution to shear capacity, various models have been proposed in the technical literature [20, 43-47]. However, since significant regions of the member cross-section are affected by confinement pressure from the steel strips and their interaction with stirrups as functions of eccentricity, the aforementioned models do not appear fully efficient.

In the present study, the shear model proposed by Shayanfar and Akbarzadeh Bengar [19] which determines the concrete shear capacity based on fiber analysis, has been extended to compute the concrete contribution to shear capacity in an RC member strengthened with a steel angle and steel strip system. By adopting Mohr's circle theory, the principal compressive (σ_c) and tensile (σ_t) stresses in an element under normal (axial) stress σ and shear stress ν of the RC member cross-section (Fig. 7) can be determined by Eqs. 42 and 43.

$$\sigma_c = \frac{\sigma}{2} + \sqrt{\frac{\sigma^2}{4} + \nu^2} \le f_{cc} \tag{42}$$

$$\sigma_t = \frac{\sigma}{2} - \sqrt{\frac{\sigma^2}{4} + \nu^2} \le f_t \tag{43}$$

Here, f_{cc} and f_t represent the compressive and tensile failure surfaces, respectively, which have been defined based on the model proposed by Park et al. [48] and the Rankine failure criterion. The tensile strength f_t has been taken equal to $f_t = 0.292\sqrt{f'_c}$ according to the study conducted by Shayanfar and Akbarzadeh Bengar [19].

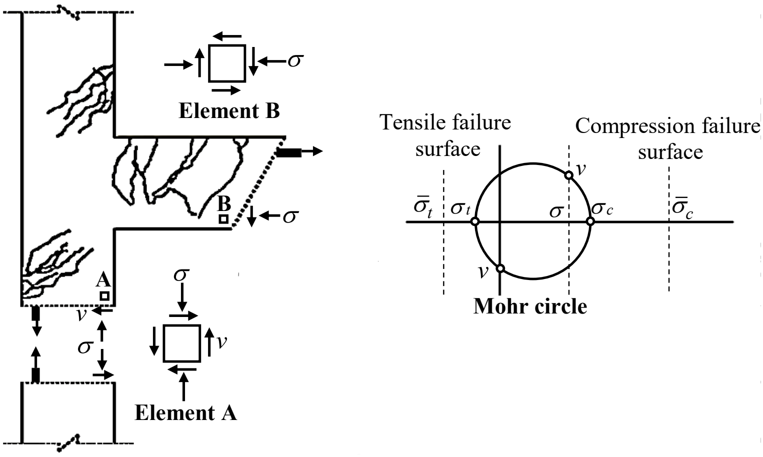

Fig. 7. Rankine failure criteria adopted for concrete.

By rewriting Eqs. 42 and 43, the shear stress capacity of an element located in the compression zone of the section can be expressed as shown in Eqs. 44 to 46.

$$v_c(y_i) = \sqrt{\sigma_c[\sigma_c - \sigma(y_i)]} \quad \text{Contributed by compression} \tag{44}$$

$$v_t(y_i) = \sqrt{\sigma_t[\sigma_t + \sigma(y_i)]} \quad \text{Contributed by tension} \tag{45}$$

$$v_n = \sum v(y_i) = \sum min\left(\sqrt{\sigma_t[\sigma_t + \sigma(y_i)]}, \sqrt{\sigma_c[\sigma_c - \sigma(y_i)]}\right) \tag{46}$$

where y_i is the distance of each element within the compression zone from the neutral axis c, which is determined through fiber section analysis. The shear stress capacity contribution of concrete in each strip of the compression zone, $v(y_i)$, is taken as the smaller value between $v_{c,i}(y_i)$ and $v_{t,i}(y_i)$. Accordingly, for each assumed neutral axis depth, the total shear strength of the RC member (considering the contributions of concrete, steel angles, steel batten, and transverse reinforcement) can be determined as shown in Eq. 47.

$$V_n = \sum v(y_i) \times b \times t_y\Big]_{Concrete} + c_1 \frac{L_1{}^2 \times t_1}{2 \times s_b} f_{ya}\Big]_{Angle} + c_2 \frac{2L_2 \times t_2 \times d}{s_b} f_{yb}\Big]_{Batten} + \frac{A_{sv} f_{sy} d_s}{s}\Big]_{Stirrup} \tag{47}$$

where t_y denotes the thickness of each fiber element in the vertical direction.

To define the plastic hinge properties of RC members while accounting for shear mechanism effects, the shear contribution is incorporated into the flexural moment-rotation relationship by multiplying the shear capacity by the shear span, L (Eq. 48).

$$M_n = V_n \times L \tag{48}$$

Using this approach, the influence of shear can be introduced into the member's flexural moment-rotation response. Fig. 8 illustrates the interaction between nonlinear flexural and shear behaviors in RC members, both strengthened and unstrengthened. As shown in the figure, the shear capacity of the member is a function of its rotation; specifically, with increasing member rotation, the shear capacity decreases. Furthermore, three distinct nonlinear behavioral modes (flexural failure, flexural-shear failure, and shear failure) can be determined by comparing the shear and flexural capacities of the member. Therefore, through the aforementioned procedure, the effects of the shear mechanism in RC members can be simulated by means of an equivalent flexural plastic hinge or a rotational spring model.

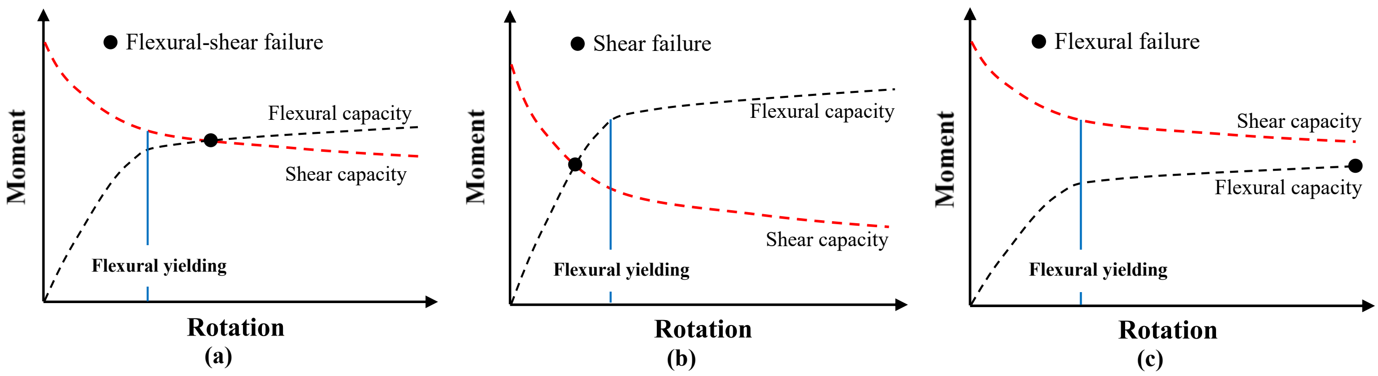

Fig. 8. Interaction between flexural and shear behaviors: (a) shear failure; (b) flexural-shear failure; and (c) flexural failure.

3.5. Longitudinal reinforcement buckling

In this section, a procedure is presented to simulate the effects of longitudinal reinforcement buckling on the seismic response of an RC member strengthened with a steel angle and steel strip system. In this paper, the model proposed by Berry and Eberhard [49] has been adopted to simulate longitudinal bar buckling. According to this model, the maximum rotation capacity of an RC member is governed by the onset of longitudinal reinforcement buckling. The steel angle and strip strengthening system, similar to transverse reinforcement (stirrups), can act as a lateral restraint for the longitudinal bars, thereby delaying the buckling mechanism [50]. In this study, the Berry and Eberhard [49] buckling model has been extended to account for the influence of steel angles and strips on the buckling phenomenon. Accordingly, the plastic rotation at the onset of longitudinal bar buckling can be determined by Eq. 49.

$$\theta_{p\_bb} = C_0\left(1 + C_1\rho_{eff,f}\right)\left(1 + C_2\frac{N}{A_g f'_c}\right)^{-1}\left(1 + C_3\frac{L}{h} + C_4\frac{f_y d_b}{h}\right) \tag{49}$$

where:

$$\rho_{eff,j} = \frac{f_{yv}\rho_s + 0.85 f_{yb}\rho_{s,b}}{f_c} \tag{50}$$

In these expressions, C_0, C_1, C_2, C_3, and C_4 are constants proposed by Berry and Eberhard [49], equal to 0.019, 1.65, 1.797, 0.012, and 0.072, respectively. The parameters ρ_s and $\rho_{s,b}$ denote the volumetric ratios of stirrups and steel strips, respectively. The coefficient 0.85 in Eq. 50 reflects the relatively lower effectiveness of the external steel angle-strip strengthening system compared with internal stirrups in restraining longitudinal bar buckling, due to its installation outside the section core. Finally, the ultimate rotation of the strengthened member corresponding to longitudinal reinforcement buckling can be calculated by Eq. 51.

$$\theta_{bb} = \frac{\varphi_y L}{2} + \theta_{p\_bb} \tag{51}$$

Therefore, the ultimate rotation capacity of the RC member can be controlled by the aforementioned buckling criterion.

3.6. Ultimate conditions of nonlinear analysis

In this section, the criteria considered in this paper for defining the ultimate conditions of the nonlinear analysis of an RC member are described. To perform the moment-curvature analysis in accordance with the proposed model, it is necessary to define termination criteria at which the nonlinear analysis is stopped. In this paper, the stopping criteria are defined as follows:

1. When the longitudinal strain of concrete at the extreme fiber of the confined compression zone reaches the ultimate longitudinal strain of confined concrete, the moment-curvature analysis is terminated.
2. When the longitudinal strain in the tensile longitudinal reinforcement reaches the maximum steel strain, the moment-curvature analysis is terminated.
3. When the longitudinal strain in the tensile steel angles reaches the maximum steel strain, the moment-curvature analysis is terminated.
4. In the case of shear failure, based on the studies by Williams and Sexsmith [51] and Park et al. [48], the maximum member rotation corresponds to 80% of the maximum member strength at the intersection point of the shear and flexural capacity curves.
5. If a reduction greater than 20% occurs in the flexural capacity of the member, the moment-curvature analysis is terminated.
6. When the member rotation exceeds the longitudinal reinforcement buckling limit, the moment-curvature analysis is terminated.

Thus, by employing the above criteria, the ultimate conditions for terminating the moment-curvature analysis can be defined.

4. Validation of the proposed model for nonlinear behavior of strengthened columns

For validation purposes, the experimental study conducted by Li et al. [52] on RC columns strengthened with a steel angle and steel strip system under constant axial load was utilized. The tested columns had a concrete compressive strength of 32.7 MPa. The experimental program included specimens strengthened using a steel jacket composed of steel angles at the corners connected by transverse steel strips. The applied axial loads ranged from 180 kN to 420 kN, corresponding to axial load ratios between 0.13 and 0.29. Two types of steel angles were used in the strengthening scheme: Angle 1 (40 × 40 × 4 mm, yield strength 350 MPa) and Angle 2 (30×30×3 mm, yield strength 338.5 MPa). Angle 2 was used only in specimen B223, while the remaining strengthened specimens utilized Angle 1. The steel strips had a cross-section of 30 × 3 mm with a yield strength of 533.3 MPa. The longitudinal reinforcement consisted of 14-mm diameter bars with a yield strength of 384.8 MPa, while the transverse reinforcement consisted of 8-mm diameter stirrups with a yield strength of 326.9 MPa. All tested specimens exhibited flexural failure modes. Further details regarding specimen geometry and test configuration are provided in Li et al. [52]. To validate the proposed nonlinear model, the predicted moment-axial force interaction diagrams were compared with the experimental results reported by Li et al. [52] in Fig. 9. The comparison indicates good agreement between analytical predictions and experimental data for different axial load levels. This consistency confirms the reliability of the proposed modeling approach and supports the assumptions adopted in the nonlinear analysis of RC members strengthened with the steel angle and strip system.

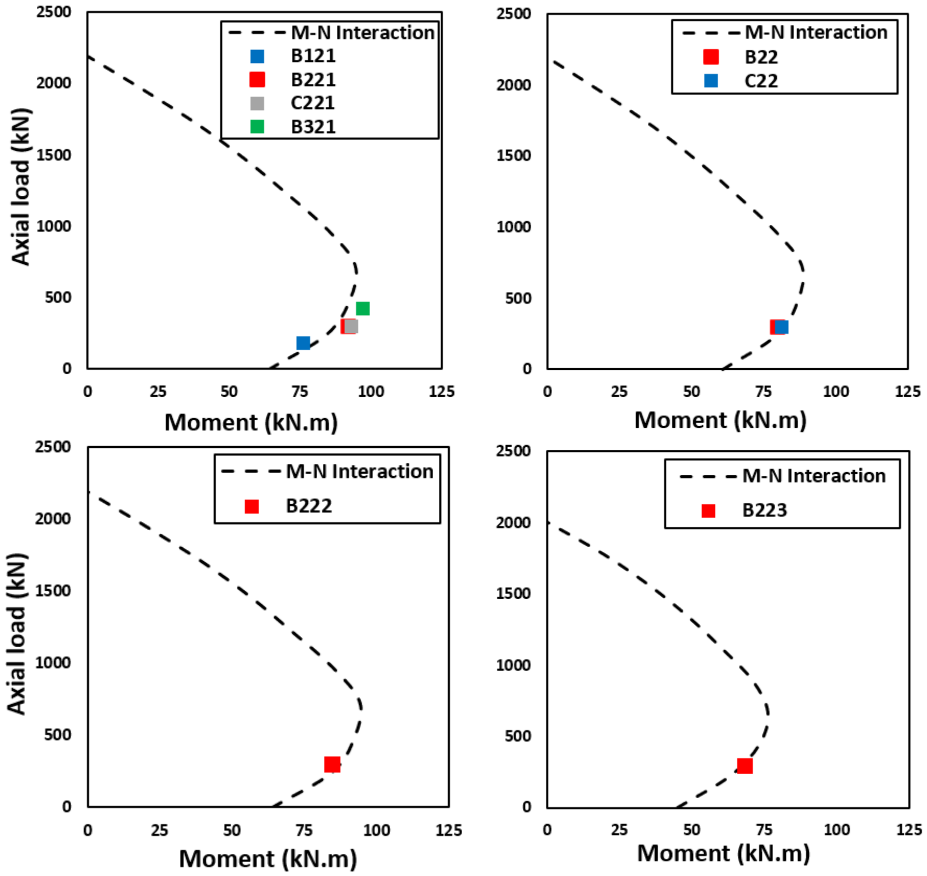

Fig. 9. Results of the nonlinear model for the column specimens tested by Li et al. [52].

Nagaprasad et al. [14] conducted experimental tests on steel-jacketed RC columns subjected to constant axial load and lateral loading. The specimens were strengthened using a steel angle and strip configuration, and all exhibited flexural failure. The concrete compressive strength was reported as 37.7 MPa. The experimental program included measurements of material properties for longitudinal reinforcement, transverse reinforcement, and the steel strengthening components, which were used to characterize the mechanical behavior of the specimens. Further experimental details are available in Nagaprasad et al. [14]. To validate the proposed nonlinear model, analytical predictions were compared with the experimental results.

As shown in Fig. 10, the moment-axial force interaction diagrams generated by the model showed satisfactory agreement with the test data across different loading conditions. This consistency confirms the capability of the model to capture the nonlinear response of strengthened RC columns and supports the assumptions adopted in the analytical formulation. The validation results demonstrate the reliability of the proposed modeling approach for predicting the behavior of members strengthened with steel angle and strip systems under combined axial and lateral loading.

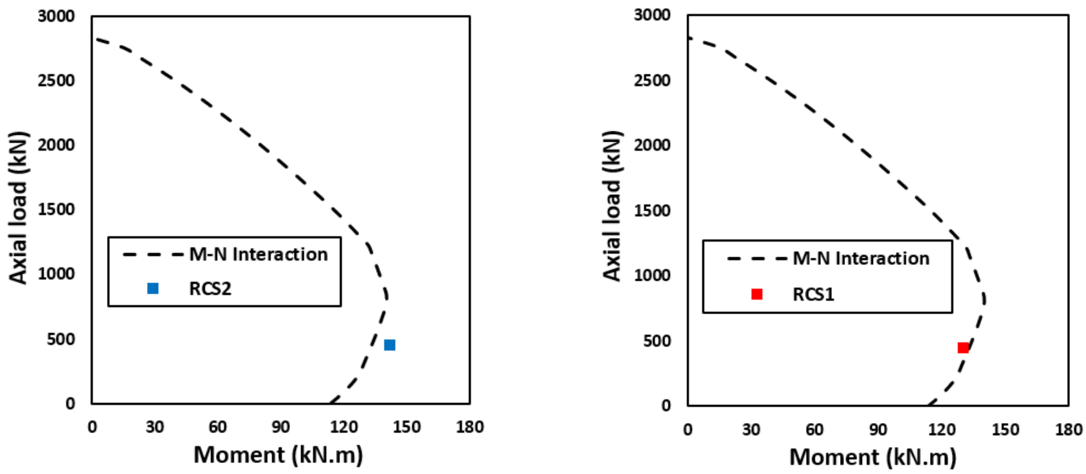

Fig. 10. Comparison between nonlinear analysis results and experimental data reported by Nagaprasad et al. [14].

Germano et al. [53] conducted experimental tests on RC columns subjected to constant axial load and lateral displacement. The specimens differed in transverse reinforcement detailing (types A and C) to investigate the influence of stirrup configuration on structural response. The columns had a height of 1800 mm and a shear span of 1565 mm, and all specimens exhibited flexural failure. Experimental load-displacement responses were reported and used for model validation. Based on Fig. 11, the comparison between analytical predictions and test results demonstrates satisfactory agreement in terms of lateral stiffness, peak resistance, and displacement capacity. The nonlinear model successfully captures the overall load-displacement behavior and seismic response characteristics of the tested columns. Although minor deviations were observed in the prediction of initial stiffness for one specimen, the model provides reliable estimations of ultimate strength and ductility. These results confirm the applicability of the proposed analytical approach for assessing the nonlinear behavior of RC columns under lateral loading conditions.

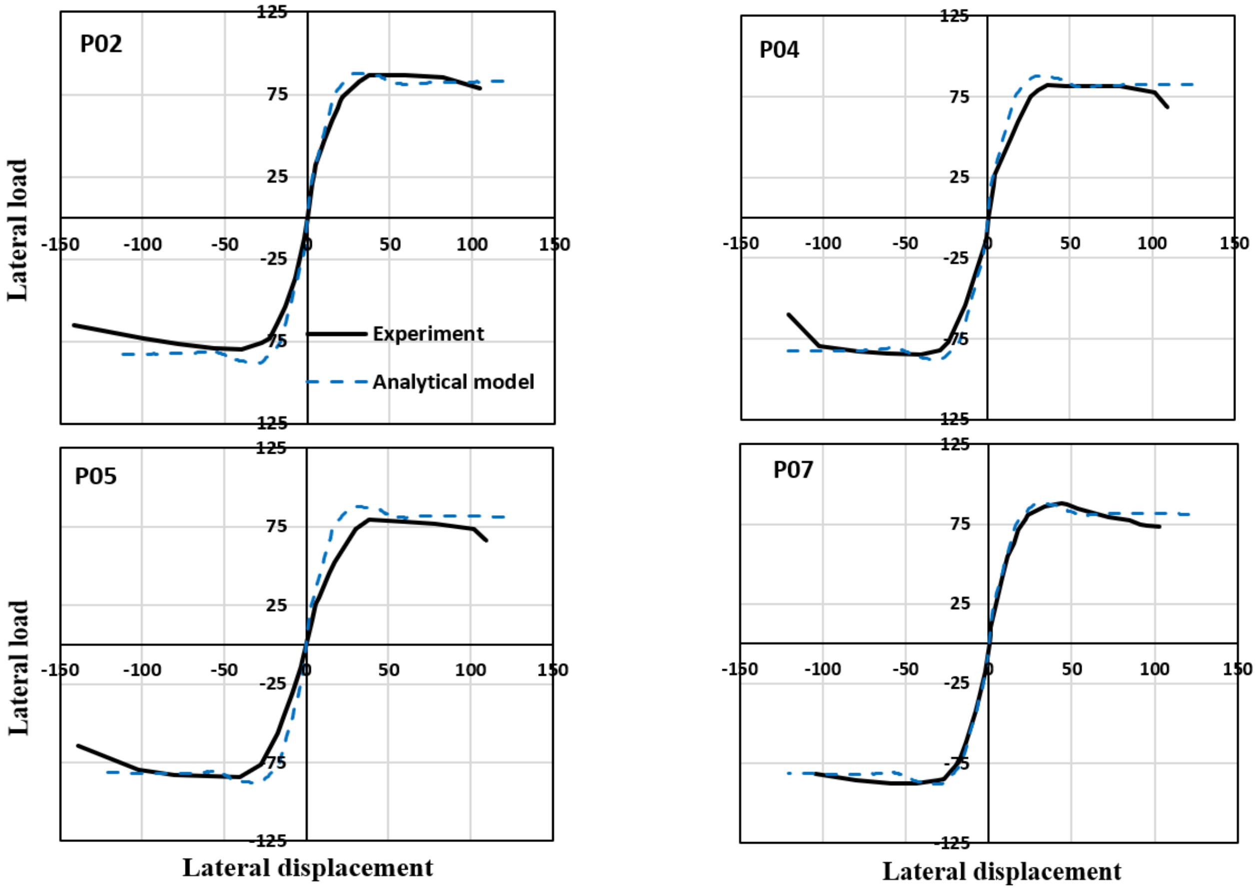

Fig. 11. Load-displacement results from nonlinear analysis compared with experimental data for column specimens tested by Germano et al. [53].

A single-span, two-storey reinforced concrete frame with a fixed base was experimentally studied by Duong et al. [54]. Lateral displacement was imposed at the second-storey beam to evaluate seismic behavior. The concrete compressive strength was measured as 42.9 MPa, and further experimental details are available in the original publication. For validation of the analytical procedure, nonlinear simulations were performed using two modeling approaches: (I) a model in which shear effects were neglected, and member response was assumed to be governed solely by flexure, and (II) a model incorporating shear effects according to the procedure adopted in this study. Based on Fig. 12, the comparison of numerical and experimental load-displacement responses indicates satisfactory agreement when shear effects are included, with the model accurately capturing stiffness degradation and ultimate displacement capacity. Conversely, exclusion of shear effects resulted in significant discrepancies in the predicted structural response. Both strength and ductility were inadequately represented, and the experimentally observed failure mechanisms – shear failure in the beams and flexural cracking in the columns – could not be reproduced with sufficient accuracy. These results demonstrate that consideration of shear effects is essential for realistic simulation of nonlinear behavior and failure modes in RC frames.

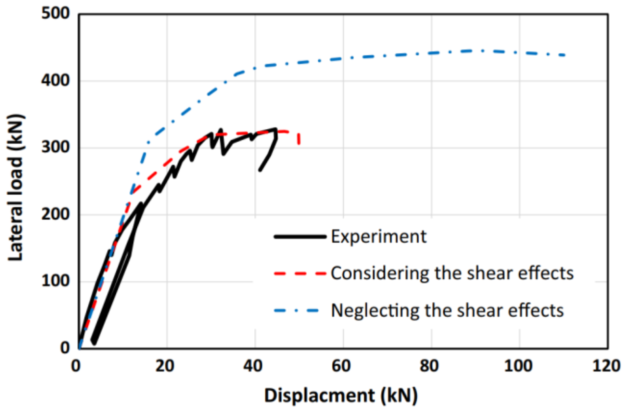

Fig. 12. Comparison of force-displacement responses of the frame: experimental results (Duong et al. [54]) and numerical analysis.

5. Evaluation of the steel angle and strip strengthening system at the structural level

In this section, the influence of the steel angle and strip strengthening system on the seismic performance of reinforced concrete structures is investigated. Three RC frame structures with four, six, and eight stories and three spans were designed, each with a story height of 3 m and a span width of 5 m. The configurations of the four-, six-, and eight-story frames (denoted as frames A, B, and C, respectively) are illustrated schematically in Fig. 13. The structural design was carried out in accordance with the Iranian seismic code, adopting standard equivalent static procedures for seismic load determination, with a lateral force distribution consistent with an inverted triangular pattern along the height of the structures. In the design process, the total dead load and a representative portion of the live load were considered in combination with the seismic loads, and member stiffness properties were defined in line with standard reinforced concrete design provisions (e.g., ACI-based practice). A notable characteristic of these structures is the relatively large spacing between transverse reinforcement (stirrups), which results in reduced confinement of the concrete core. The dimensions and reinforcement details for the beam and column sections (sections A-F) are summarized in Table 1. The notations $A_{s,top}$ and A_s, bot represent the areas of reinforcement at the top and bottom of the beam sections, respectively. The longitudinal reinforcement arrangement is specified as 16 bars of 25 mm diameter (denoted as n16φ25). The concrete compressive strength and the yield and ultimate strengths of the longitudinal and transverse reinforcement were taken as 25 MPa, 420 MPa, and 650 MPa, respectively. The diameter of the stirrups was 10 mm, consistent with the reinforcement details provided in Table 1. In all stories, three layers of stirrups were provided in the beam-column joint regions to enhance confinement and mitigate diagonal cracking within the joint core. Based on previous studies [3, 55], this reinforcement detailing is sufficient to improve shear resistance and reduce joint damage, thereby justifying the assumption of rigid joint behavior in the analysis. The seismic design of the frames was based on a design ground acceleration of 0.3 g and soil type III, corresponding to a high seismic hazard zone. The base shear was determined in accordance with the seismic design provisions. Dead and live loads were considered as 30 kN/m and 10 kN/m, respectively, in the structural design. This structural configuration enables evaluation of the effectiveness of the steel angle and strip strengthening system in enhancing seismic performance and mitigating damage under lateral loading conditions.

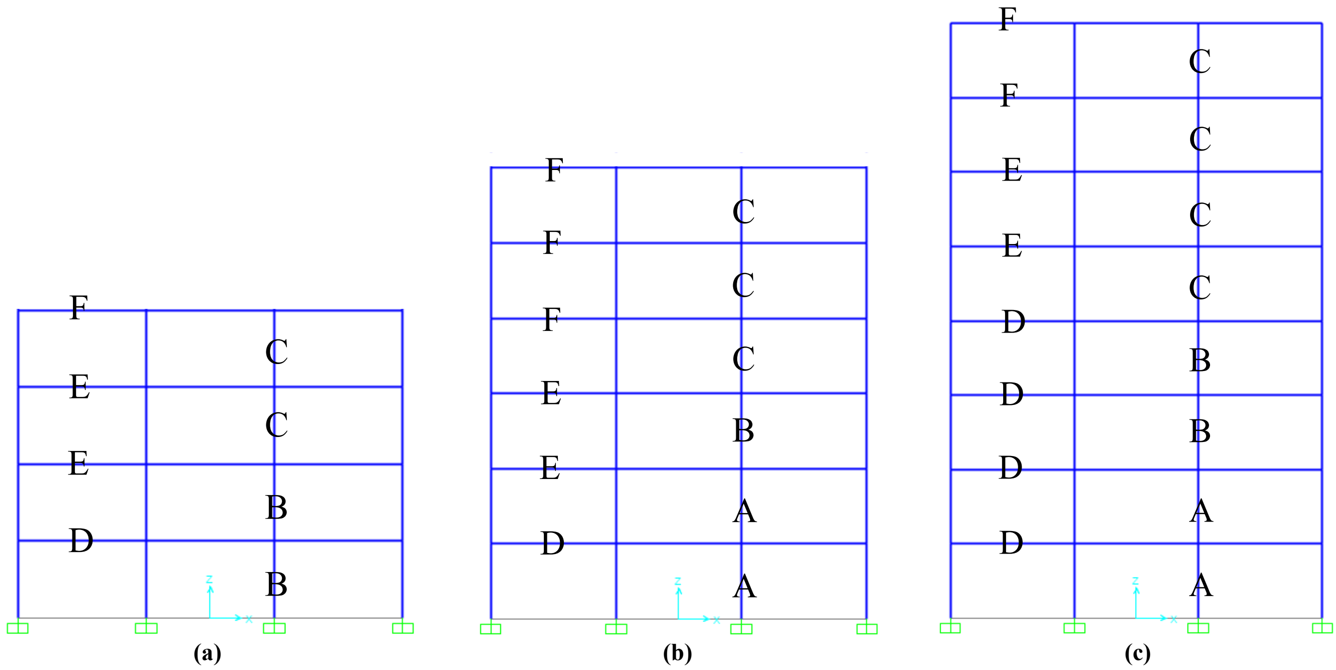

Fig. 13. Geometric configuration of the studied structures: (a) four-story frame (frame A); (b) six-story frame (frame B); and (c) eight-story frame (frame C).

In the nonlinear analysis performed in SAP2000 Version 20.2.0 [56], the plastic hinges assigned to beams and columns were defined as user-defined hinges based on the proposed analytical model. Specifically, M3 hinges were assigned to beam elements and P-M3 interaction hinges were assigned to column elements. Although these hinges are classified as flexural hinges, their defining properties were derived from the proposed model, which inherently incorporates the influence of shear behavior, confinement effects, and material nonlinearities in the moment-curvature response used to define hinge properties. The hinges were located at a distance equal to 50% of the plastic hinge length from the element ends, which is consistent with common modeling practice to represent the development of inelastic rotations away from the critical section. The hinge behavior, including yield and post-yield characteristics, was directly informed by the analytical formulation presented in the study, ensuring consistency between the sectional modeling and the global structural response. In the studied frames, the strengthening strategy is focused on improving the seismic performance of the structure and enhancing nonlinear behavior at the locations of plastic hinge formation. Tables 2 to 4 present the details of the steel angles and steel strips designed for the four-, six-, and eight-story frames.

Fig. 14 illustrates an example of the steel angle and strip configuration in frame F, first story, at an interior beam-column joint. It should be noted that in all members, the spacing of steel strips within the plastic hinge region was designed as 200 mm, while outside this region it was increased to 350 mm. The strengthening system was designed as a continuous configuration in all frames, allowing the steel angles to contribute to both tensile and compressive load transfer. This continuity enhances the flexural capacity of the members and improves overall seismic performance.

Table 1. Dimensions and reinforcement details of sections (A to F).

Section	Type	b (mm)	h (mm)	A_{st}	$A_{s,top}$	$A_{s,bot}$	Stirrup
A-A	Column	600	600	n16φ25	–	–	d10@450
B-B	Column	–	–	n16φ18	–	–	–
C-C	Column	500	500	n16φ16	–	–	–
D-D	Beam	–	–	–	n4φ25	n6φ25	d10@140
E-E	Beam	–	–	–	n4φ22	n6φ22	d10@175
F-F	Beam	–	–	–	n3φ18	n6φ18	d10@250

Table 2. Steel angle and strip details for frame D.

Story	External angle (beam)	External angle (column)	External strip (beam)	External strip (column)	Internal angle (beam)	Internal angle (column)	Internal strip (beam)	Internal strip (column)
1	4 × 40 × 40	6 × 60 × 60	4 × 40	5 × 50	4 × 40 × 40	6 × 60 × 60	4 × 40	5 × 50
2	–	8 × 80 × 80	–	7 × 70	–	8 × 80 × 80	–	7 × 70
3	–	3 × 30 × 30	–	3 × 30	–	5 × 50 × 50	–	5 × 50
4	–	3 × 30 × 30	–	3 × 30	–	3 × 30 × 30	–	3 × 30

Table 3. Steel angle and strip details for frame E.

Story	External angle (beam)	External angle (column)	External strip (beam)	External strip (column)	Internal angle (beam)	Internal angle (column)	Internal strip (beam)	Internal strip (column)
1	–	5 × 50 × 50	–	4 × 40	–	5 × 50 × 50	–	4 × 40
2	4 × 40 × 40	4 × 40 × 40	4 × 40	3 × 30	4 × 40 × 40	5 × 50 × 50	4 × 40	4 × 40
3	4 × 40 × 40	4 × 40 × 40	4 × 40	3 × 30	4 × 40 × 40	4 × 40 × 40	4 × 40	3 × 30
4	4 × 40 × 40	4 × 40 × 40	4 × 40	3 × 30	4 × 40 × 40	4 × 40 × 40	4 × 40	3 × 30
5	–	4 × 40 × 40	–	3 × 30	–	4 × 40 × 40	4 × 40	3 × 30
6	–	–	–	–	–	–	–	–

Table 4. Steel angle and strip details for frame F.

Story	External angle (beam)	External angle (column)	External strip (beam)	External strip (column)	Internal angle (beam)	Internal angle (column)	Internal strip (beam)	Internal strip (column)
1	4 × 40 × 40	7 × 70 × 70	4 × 40	6 × 60	4 × 40 × 40	5 × 50 × 50	5 × 50	4 × 40
2	5 × 50 × 50	4 × 40 × 40	5 × 50	3 × 30	5 × 50 × 50	4 × 40 × 40	4 × 40	3 × 30
3	5 × 50 × 50	4 × 40 × 40	5 × 50	3 × 30	5 × 50 × 50	4 × 40 × 40	4 × 40	3 × 30
4	5 × 50 × 50	4 × 40 × 40	5 × 50	3 × 30	5 × 50 × 50	4 × 40 × 40	4 × 40	3 × 30
5	4 × 40 × 40	4 × 40 ×40	4 × 40	3 × 30	4 × 40 × 40	4 × 40 × 40	4 × 40	3 × 30
6	4 × 40 × 40	4 × 40 × 40	4 × 40	3 × 30	4 × 40 × 40	5 × 50 × 50	5 × 50	4 × 40
7	–	–	–	–	–	–	–	–
8	–	–	–	–	–	–	–	–

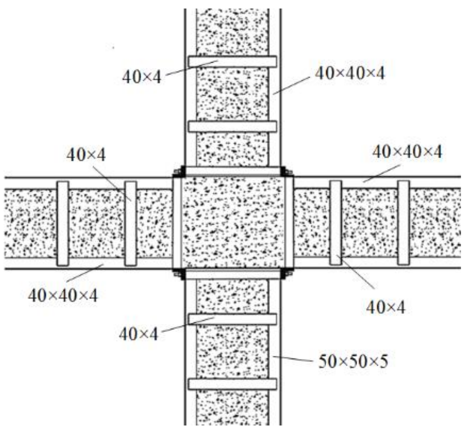

Fig. 14. Example of the steel angle and strip strengthening configuration in frame F, first story, interior beam-column joint.

In this sense, the geometry and mechanical properties of the strengthening elements are not arbitrary inputs, but are the direct outcome of a performance-driven design process. It should be emphasized that there is no unique or closed-form solution for selecting the strengthening layout, as the response depends on load distribution, members' capacity, and the interaction between confinement, flexural resistance, and shear capacity at both member and structural levels. Therefore, the adopted iterative approach represents a rational and standard methodology in performance-based seismic design, ensuring that the final configuration is both efficient and consistent with the targeted performance objective.

5.1. Seismic behavior of structures A to F

In this section, the nonlinear response and seismic performance of the RC structures (Frames A to F) are evaluated before and after strengthening with the steel angle and shear strip system. The parameters of interest include the load-displacement behavior, seismic performance, and plastic hinge formation patterns at the performance point and ultimate deformation state. Nonlinear static analysis was conducted using SAP2000 Version 20.2.0 [56], and plastic hinges were defined in accordance with the procedures described in this study. A triangular lateral load distribution was applied. Fig. 15 presents the results of nonlinear analysis in terms of lateral load-displacement response and the distribution of plastic hinges at the ultimate state. For the four-story frame, the results indicate that frame A exhibits improved strength and ductility after strengthening.

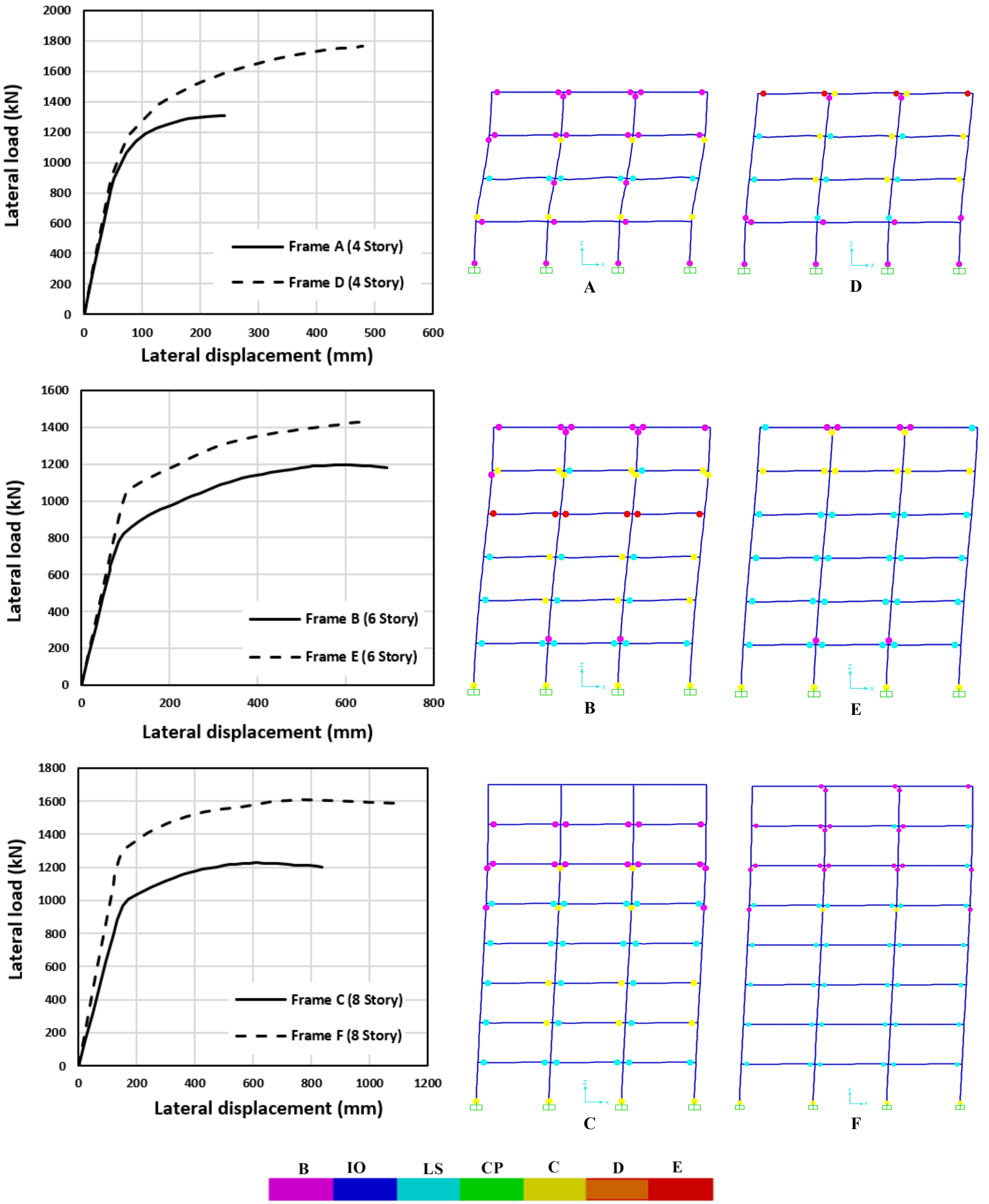

Fig. 15. Load-displacement response and corresponding damage pattern at the ultimate state.

The damage pattern shows that plastic hinges form in all columns prior to strengthening, with rotations in the second and third stories being more pronounced. This suggests the possibility of a soft-story mechanism in these regions. Following strengthening, plastic hinges predominantly form in the beams, while hinge rotations in the columns of the second and fourth stories are reduced and remain well below their ultimate limits.

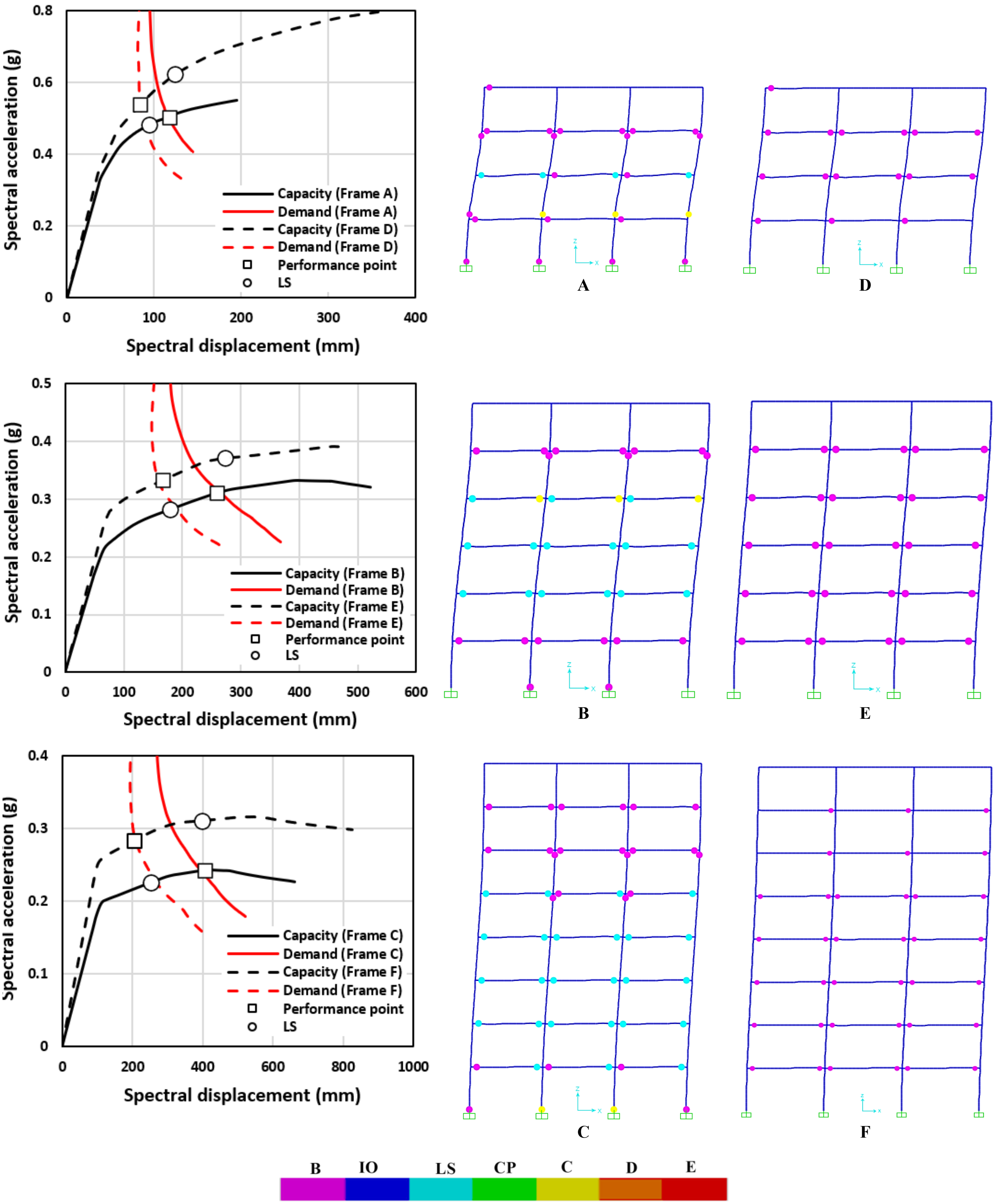

Fig. 16. Spectral acceleration-spectral displacement results and the damage pattern corresponding to the performance point.

Although the maximum lateral displacement of the strengthened frame exceeds that of the unstrengthened configuration, the post-strengthening hinge distribution reflects a more favorable failure mechanism. In the six-story frame, strengthening improved lateral stiffness and initial strength. However, the maximum lateral displacement in the strengthened configuration was slightly lower than in the original frame. The damage pattern indicates that plastic hinge rotations in the fifth-story columns approached their ultimate limits, increasing the likelihood of a soft-story mechanism. To address this, the strengthening strategy prioritized column enhancement while avoiding excessive stiffening of adjacent beams, thereby encouraging plastic hinge formation in beams rather than columns. After strengthening, plastic hinges predominantly developed in beams, while column hinge rotations were limited to yield-level deformations in the second story and remained moderate in the top story where strengthening was not applied. For the eight-story frame, strengthening resulted in improved strength, ductility, and initial stiffness. The damage pattern revealed that plastic hinge rotations in the fifth and sixth stories approached ultimate limits, indicating a potential soft-story mechanism in these regions. After strengthening, hinge formation was primarily observed in the beams, while column rotations in the critical stories were reduced. Although the maximum lateral displacement of the strengthened frame remained greater than that of the unstrengthened frame, the plastic hinge distribution and failure pattern were significantly improved.

Fig. 16 illustrates the nonlinear analysis results with respect to seismic performance and plastic hinge distribution at the performance point. Seismic performance is assessed by comparing the performance point with the life safety (LS) performance level, as defined in FEMA 356 [57]. At the LS level, structural and nonstructural components experience moderate damage and deformation. Lateral stiffness and the ability to resist additional lateral loads are reduced, and while collapse is unlikely, the structure may no longer be suitable for immediate occupancy. Repair may be possible but is often not economically practical. For the four-story frame, frame A remained beyond the LS performance level, indicating limited seismic performance in its original configuration. The hinge distribution confirmed the likelihood of a soft-story mechanism in the second story. After strengthening, plastic hinges formed primarily in the beams and remained within yield-level rotations, well below the LS limit. No significant hinge formation occurred at the base of the structure. The results in terms of load-displacement response, seismic performance, and hinge distribution at the performance point confirm the effectiveness of the steel angle and strip strengthening system in improving seismic behavior. In the four-story configuration, frame B remained beyond the life safety (LS) performance level, indicating inadequate seismic performance under design-level earthquakes. The plastic hinge distribution suggests the possibility of a soft-story mechanism in the fifth story, while hinge rotations in the fourth-story beams approached their ultimate limits.

After strengthening, plastic hinges were primarily confined to the beams and remained within yield-level rotations, with considerable margin from the LS threshold. The load-displacement response, seismic performance, and plastic hinge distribution at the performance point and ultimate deformation confirm the effectiveness of the steel angle and strip strengthening system. Similarly, in the four-story configuration, frame C also remained beyond the LS performance level, reflecting limited seismic performance in its unstrengthened state. The damage pattern indicated potential soft-story behavior in the fifth and sixth stories, and column hinge rotations at the base of the structure approached their ultimate limits. Following strengthening, plastic hinges developed predominantly in the beams, with rotations remaining within the yield range and far from the LS limit. The results in terms of structural response, seismic performance, and hinge formation at the performance point validate the effectiveness of the strengthening strategy using the steel angle and strip system.

It is noteworthy that the proposed model is developed within a nonlinear static (monotonic) framework; however, its formulation is based on sectional constitutive relationships that are inherently suitable for extension to cyclic and dynamic analyses. For application under cyclic loading, the model would require the incorporation of appropriate hysteretic rules to capture unloading-reloading behavior, stiffness and strength degradation, and energy dissipation. Similarly, for dynamic analysis, the model can be implemented within a time-history framework by integrating the proposed nonlinear hinge properties into the structural model along with suitable damping definitions. These extensions are straightforward and consistent with the fiber-based formulation adopted in this study.

6. Conclusions

This study focused on evaluating the nonlinear behavior and seismic performance of reinforced concrete (RC) structures and their strengthening using a steel angle and strip system. Analytical procedures were developed to capture nonlinear mechanisms before and after strengthening, enabling a rigorous assessment of seismic response. A modeling framework was proposed to incorporate the effects of the strengthening system on seismic behavior. The strengthening strategy influences nonlinear response through longitudinal strain development in the steel angles, allowing them to resist tensile and compressive forces and contribute to load transfer. Possible buckling of steel angles in compression zones was also included in the nonlinear formulation to represent realistic structural behavior. Furthermore, the combined action of steel strips and angles provides confinement to the concrete core, and this confinement effect was considered in the moment-curvature analysis of strengthened members. Insufficient shear capacity in RC members can lead to brittle shear failure and increased seismic vulnerability. Diagonal shear cracking in columns may reduce axial load-carrying capacity, while large flexural deformations and diagonal tensile cracking can further diminish shear resistance. Nonlinear analysis that neglects shear mechanisms may produce unconservative predictions of strength and deformation capacity, highlighting the necessity of incorporating shear effects in performance-based assessment. For strengthened members, a shear model was developed that considers contributions from stirrups, concrete, steel angles, and strips to overall shear capacity. Four-, six-, and eight-story RC frames were designed and strengthened to evaluate seismic performance. The results demonstrated close agreement between analytical predictions and experimental data, confirming the capability of the proposed model to simulate flexural and shear behavior under different loading conditions. Strengthening with the steel angle and strip system significantly improved initial stiffness, load-carrying capacity, and ductility. Load-displacement results of strengthened frames showed that the strengthening system enhances initial stiffness and seismic resistance when properly designed. Additionally, plastic hinge formation was redirected from columns to beams, mitigating undesirable strong-beam-weak-column mechanisms and improving overall structural performance. Seismic performance evaluation indicated that strengthening can shift the performance point toward a more favorable state and reduce damage potential at critical locations. The findings confirm that the steel angle and strip strengthening system is an effective strategy for improving nonlinear response and seismic performance of RC structures when appropriately designed and implemented.

Statements & declarations

Author contributions

Hananeh Dashtaki: Investigation, Formal analysis, Data curation, Software, Validation, Writing - Original Draft.

Javad Shayanfar: Conceptualization, Methodology, Software, Writing - Review & Editing.

Morteza Jamshidi: Project administration, Resources, Supervision, Writing - Review & Editing.

Acknowledgments

The authors declare that there are no acknowledgments to report for this work.

Funding

Funding information is not available.

Data availability

All data are available in the manuscript.

Declarations

The authors declare no conflict of interest.

References

[1] Sadeghpour Haji, M., Niknam, R., Shayanfar, J. ANN-Based Modeling of Shear Behavior of Reinforced Concrete Columns under Constant Axial Loads. Civil Engineering and Applied Solutions, 2026; 2: 28–48. doi:10.22080/ceas.2025.30228.1050.

[2] Abedi, M., Fangueiro, R., Correia, A. G., Shayanfar, J. Smart Geosynthetics and Prospects for Civil Infrastructure Monitoring: A Comprehensive and Critical Review. Sustainability, 2023; 15: 9258. doi:10.3390/su15129258.

[3] Shayanfar, J., Hemmati, A., Bengar, H. A. A simplified numerical model to simulate RC beam–column joints collapse. Bulletin of Earthquake Engineering, 2019; 17: 803–844. doi:10.1007/s10518-018-0472-z.

[4] Mohammadi, A., Shayanfar, J., Barros, J. A. O. Reliability-based design model for compressive strength of axially loaded FRP-confined concrete columns. Composite Structures, 2026; 384: 120159. doi:10.1016/j.compstruct.2026.120159.

[5] Shayanfar, J., Baharloo, S., Barros, J. A. O., Mohammadi, A. Strength Model for FRP-Confined Concrete: Comprehensive Database and Reliability-Based Partial Factor Calibration. Journal of Composites for Construction, 2026; 30: 04026006. doi:10.1061/JCCOF2.CCENG-5448.

[6] Salman, H. M., Al-Sherrawi, M. H. M-N Interaction Diagrams of RC Columns Strengthened with Steel C-Sections and Battens. Civil Engineering Journal, 2024; 10: 1974–1986. doi:10.28991/CEJ-2024-010-06-016.

[7] Abedi, M., Shayanfar, J., Al-Jabri, K. Infrastructure damage assessment via machine learning approaches: a systematic review. Asian Journal of Civil Engineering, 2023; 24: 3823–3852. doi:10.1007/s42107-023-00748-5.

[8] Erange, Y. G. P., Jenothan, M., Jayasinghe, J. A. S. C., Bandara, C. S., Dammika, A. J. Enhancement of the Lateral Performance of RC Columns Using Steel Jacketing: A Numerical Approach. Engineer: Journal of the Institution of Engineers, Sri Lanka, 2023; 56: 51–64. doi:10.4038/engineer.v56i2.7576.

[9] Shhatha, M. A., Mahdi, W. H., Alalikhan, A. A. Assessment for behavior of axially loaded reinforced concrete columns strengthened by different patterns of steel-framed jacket. Open Engineering, 2023; 13: 20220414. doi:10.1515/eng-2022-0414.

[10] Hu, Q., Jia, S., Wu, H., Wang, T. Experimental Research of Axial Compression Bearing Capacity on RC Columns Strengthened with Angle Steel and Self-Compacting Concrete. International Journal of Steel Structures, 2022; 22: 253–262. doi:10.1007/s13296-021-00571-1.

[11] Salah, A., Elsanadedy, H., Abbas, H., Almusallam, T., Al-Salloum, Y. Behavior of axially loaded L-shaped RC columns strengthened using steel jacketing. Journal of Building Engineering, 2022; 47: 103870. doi:10.1016/j.jobe.2021.103870.

[12] Akbarzadeh Bengar, H., Abdollahtabar, M., Shayanfar, J. Predicting the Ductility of RC Beams Using Nonlinear Regression and ANN. Iranian Journal of Science and Technology, Transactions of Civil Engineering, 2016; 40: 297–310. doi:10.1007/s40996-016-0033-0.

[13] Montuori, R., Piluso, V. Reinforced concrete columns strengthened with angles and battens subjected to eccentric load. Engineering Structures, 2009; 31: 539–550. doi:10.1016/j.engstruct.2008.10.005.

[14] Nagaprasad, P., Sahoo, D. R., Rai, D. Seismic strengthening of RC columns using external steel cage. Earthquake Engineering & Structural Dynamics, 2009; 38: 1563–1586. doi:10.1002/eqe.917.

[15] Campione, G., Monaco, A., Papia, M. Simplified analytical model for moment–axial force domain in the presence of shear in R.C. members externally strengthened with steel cages. Materials and Structures, 2016; 49: 3143–3157. doi:10.1617/s11527-015-0710-7.

[16] Campione, G. Strength and ductility of R.C. columns strengthened with steel angles and battens. Construction and Building Materials, 2012; 35: 800–807. doi:10.1016/j.conbuildmat.2012.04.090.

[17] Campione, G. RC Columns Strengthened with Steel Angles and Battens: Experimental Results and Design Procedure. Practice Periodical on Structural Design and Construction, 2013; 18: 1–11. doi:10.1061/(ASCE)SC.1943-5576.0000125.

[18] Badalamenti, V., Campione, G., Mangiavillano, M. L. Simplified Model for Compressive Behavior of Concrete Columns Strengthened by Steel Angles and Strips. Journal of Engineering Mechanics, 2010; 136: 230–238. doi:10.1061/(ASCE)EM.1943-7889.0000069.

[19] Shayanfar, J., Akbarzadeh Bengar, H. Nonlinear analysis of RC frames considering shear behaviour of members under varying axial load. Bulletin of Earthquake Engineering, 2017; 15: 2055–2078. doi:10.1007/s10518-016-0060-z.

[20] Khant, K., Shayanfar, J., Nguyen, H., Rezazadeh, M. Multi-Layer Perceptron for Prediction of Axial Strength of Fully FRP-Confined Circular Concrete. In: 12th International Conference on FRP Composites in Civil Engineering (CICE 2025); 2025 Jul 14–16; Lisbon, Portugal. p. 1041–1048. doi:10.1007/978-3-032-09387-5_101.

[21] Shayanfar, J., Barros, J. A. O., Rezazadeh, M. Analysis-oriented model for partially FRP-and-steel-confined circular RC columns under compression. Engineering Structures, 2023; 276: 115330. doi:10.1016/j.engstruct.2022.115330.

[22] Shayanfar, J., Barros, J. A. O., Rezazadeh, M. Cross-sectional and confining system unification on peak compressive strength of FRP confined concrete. Structural Concrete, 2023; 24: 1531–1545. doi:10.1002/suco.202200105.

[23] Shayanfar, J., Barros, J. A. O., Rezazadeh, M. Analytical model to predict axial stress-strain behavior of heat-damaged unreinforced concrete columns wrapped by FRP jacket. Engineering Structures, 2023; 289: 116244. doi:10.1016/j.engstruct.2023.116244.

[24] Pereira, J. P. C., Shayanfar, J., Barros, J. A. O. Effect of Different Passive FRP Confinement Arrangements on Stress-Strain Behavior of Axially-Loaded Fire-Damaged Concrete Elements. In: 12th International Conference on FRP Composites in Civil Engineering (CICE 2025); 2025 Jul 14–16; Lisbon, Portugal. p. 1033–1040. doi:10.1007/978-3-032-09399-8_97.

[25] Shayanfar, J., Barros, J. A. O. Design-Oriented Model of Unified Character to Determine Softening–Hardening Stress–Strain Behavior of FRP-Confined Concrete Columns of General Cross Section. Journal of Composites for Construction, 2024; 28: 04024059. doi:10.1061/JCCOF2.CCENG-4772.

[26] Shayanfar, J., Omidalizadeh, M., Nematzadeh, M. Analysis-oriented Model for Seismic Assessment of RC Jacket Retrofitted Columns. Steel and Composite Structures, 2020; 37: 371–390. doi:10.12989/scs.2020.37.3.371.

[27] Mander, J. B., Priestley, M. J. N., Park, R. Theoretical Stress-Strain Model for Confined Concrete. Journal of Structural Engineering, 1988; 114: 1804–1826. doi:10.1061/(ASCE)0733-9445(1988)114:8(1804).

[28] Wang, Y. C., Restrepo, J. I. Investigation of concentrically loaded reinforced concrete columns confined with glass fiber-reinforced polymer jackets. Structural Journal, 2001; 98: 377–385.

[29] Nematzadeh, M., Mousavimehr, M., Shayanfar, J., Omidalizadeh, M. Eccentric compressive behavior of steel fiber-reinforced RC columns strengthened with CFRP wraps: Experimental investigation and analytical modeling. Engineering Structures, 2021; 226: 111389. doi:10.1016/j.engstruct.2020.111389.

[30] Shayanfar, J., Rezazadeh, M., Barros, J. A. Analytical Model to Predict Dilation Behavior of FRP Confined Circular Concrete Columns Subjected to Axial Compressive Loading. Journal of Composites for Construction, 2020; 24: 04020071. doi:10.1061/(ASCE)CC.1943-5614.0001087.

[31] Wang, J., Xiao, H., Lu, L., Yang, J., Lu, S., Shayanfar, J. Axial stress-strain model for concrete in partially FRP wrapped reinforced concrete columns. Construction and Building Materials, 2024; 416: 135028. doi:10.1016/j.conbuildmat.2024.135028.

[32] Shayanfar, J., Barros, J. A. O., Pereira, J. P. C. A versatile model with a design framework for axially-loaded FRP-confined concrete with/without a stress reduction-recovery behavior. Construction and Building Materials, 2024; 448: 138097. doi:10.1016/j.conbuildmat.2024.138097.

[33] Shayanfar, J., Barros, J. A. O., Rezazadeh, M. Design-oriented stress–strain model for RC columns with dual FRP- steel confinement mechanism. Composite Structures, 2024; 330: 117821. doi:10.1016/j.compstruct.2023.117821.

[34] Shayanfar, J., Barros, J. A. O., Rezazadeh, M. Stress–Strain Model for FRP-Confined Circular Concrete Columns Developing Structural Softening Behavior. Journal of Composites for Construction, 2024; 28: 04023065. doi:10.1061/JCCOF2.CCENG-4364.

[35] Shayanfar, J., Barros, J. A. O., Rezazadeh, M., Kafshgarkolaei, H. J. Enhancing the performance of heat-damaged rectangular RC columns using prestressed FRP confinement. Construction and Building Materials, 2025; 501: 144346. doi:10.1016/j.conbuildmat.2025.144346.

[36] Paulay, T., Priestly, M. J. N. Seismic Design of Reinforced Concrete and Masonry Buildings. First ed. New York (NY): John Wiley & Sons, Inc; 1992. doi:10.1002/9780470172841.

[37] Shayanfar, J., Barros, J. A., Rezazadeh, M. Unified model for fully and partially FRP confined circular and square concrete columns subjected to axial compression. Engineering Structures, 2022; 251: 113355. doi:10.1016/j.engstruct.2021.113355.

[38] Shayanfar, J., Barros, J. A. O., Rezazadeh, M. Generalized Analysis-oriented model of FRP confined concrete circular columns. Composite Structures, 2021; 270: 114026. doi:10.1016/j.compstruct.2021.114026.

[39] Shayanfar, J., Akbarzadeh Bengar, H., Niroomandi, A. A proposed model for predicting nonlinear behavior of RC joints under seismic loads. Materials & Design, 2016; 95: 563–579. doi:10.1016/j.matdes.2016.01.098.

[40] Shayanfar, J., Pereira, J. P. C., Barros, J. A. O. Passive confinement scenarios for strengthening fire-damaged concrete columns: Experimental and analytical research. Structures, 2025; 73: 108375. doi:10.1016/j.istruc.2025.108375.

[41] Abedi, M., Roshan, M. J., Gulisano, F., Shayanfar, J., Adresi, M., Fangueiro, R., Correia, A. G. An advanced cement-based geocomposite with autonomous sensing and heating capabilities for enhanced intelligent transportation infrastructure. Construction and Building Materials, 2024; 411: 134577. doi:10.1016/j.conbuildmat.2023.134577.

[42] Akbarzadeh Bengar, H., Assadikiadehi, M., Shayanfar, J., Nazari, M. Effective flexural rigidities for RC beams and columns with steel fiber. Steel and Composite Structures, 2019; 34: 453–465. doi:10.12989/scs.2020.34.3.453.

[43] Tariq, M., Khan, A., Ullah, A., Shayanfar, J., Niaz, M. Improved Shear Strength Prediction Model of Steel Fiber Reinforced Concrete Beams by Adopting Gene Expression Programming. Materials (Basel), 2022; 15: 3758. doi:10.3390/ma15113758.

[44] Tariq, M., Khan, A., Shayanfar, J., Hanif, M. U., Ullah, A. A regression model for predicting the shear strength of RC knee joint subjected to opening and closing moment. Journal of Building Engineering, 2021; 41: 102727. doi:10.1016/j.jobe.2021.102727.

[45] Shayanfar, J., Akbarzadeh Bengar, H. A practical model for simulating nonlinear behaviour of FRP strengthened RC beam-column joints Steel and Composite Structures, 2018; 27: 49–74. doi:10.12989/scs.2018.27.1.049

[46] Pan, Z., Li, B. Truss-Arch Model for Shear Strength of Shear-Critical Reinforced Concrete Columns. Journal of Structural Engineering, 2013; 139: 548–560. doi:10.1061/(ASCE)ST.1943-541X.0000677.

[47] Lynn, A. C. Seismic evaluation of existing reinforced concrete building columns [PhD Thesis]. Berkeley (CA): University of California, Berkeley; 2001.

[48] Park, H.-G., Yu, E.-J., Choi, K.-K. Shear-strength degradation model for RC columns subjected to cyclic loading. Engineering Structures, 2012; 34: 187–197. doi:10.1016/j.engstruct.2011.08.041.

[49] Berry, M. P., Eberhard, M. O. Practical Performance Model for Bar Buckling. Journal of Structural Engineering, 2005; 131: 1060–1070. doi:10.1061/(ASCE)0733-9445(2005)131:7(1060).

[50] Shayanfar, J., Akbarzadeh, B. Numerical model to simulate shear behaviour of RC joints and columns. Computers and Concrete, 2016; 18: 877–901. doi:10.12989/cac.2016.18.4.877.

[51] Williams, M. S., Sexsmith, R. G. 8. Seismic Damage Indices for Concrete Structures: A State-of-the-Art Review. Earthquake Spectra, 1995; 11: 319–349. doi:10.1193/1.1585817.

[52] Li, J., Gong, J., Wang, L. Seismic behavior of corrosion-damaged reinforced concrete columns strengthened using combined carbon fiber-reinforced polymer and steel jacket. Construction and Building Materials, 2009; 23: 2653–2663. doi:10.1016/j.conbuildmat.2009.01.003.

[53] Germano, F., Plizzari, G. A., Tiberti, G. Experimental study on the behavior of SFRC columns under seismic loads. In: VIII International Conference on Fracture Mechanics of Concrete and Concrete Structures FraMCoS-8; 2013 Mar 10–13; Toledo, Spain. p. 1–12.

[54] Duong, V., Sheikh, S., Vecchio, F. Seismic behavior of shear-critical reinforced concrete frame: Experimental investigation. ACI Structural Journal, 2007; 104: 304–313. doi:10.14359/18620.

[55] Shayanfar, J., Bengar, H. A., Parvin, A. Analytical prediction of seismic behavior of RC joints and columns under varying axial load. Engineering Structures, 2018; 174: 792–813. doi:10.1016/j.engstruct.2018.07.103.

[56] Computers and Structures, Inc. (CSI). SAP2000 Integrated Software for Structural Analysis and Design. Version 20.2.0. Berkeley (CA): Computers and Structures, Inc. (CSI); 2018.

[57] Federal Emergency Management Agency (FEMA). FEMA 356: Prestandard and Commentary for the Seismic Rehabilitation of Buildings. Washington, D.C. (US): ASCE; 2000.